AD-A148 673 PHYSICAL PROPERTIES OF THE NICKEL COMPOSITE SINTERED PLAQUE(U) NAVAL SURFACE WEAPONS CENTER SILVER SPRING MD W A FERRANDO ET AL. DEC 82 NSWC/TR-82-416 1/1

UNCLASSIFIED F/G 10/3 NL

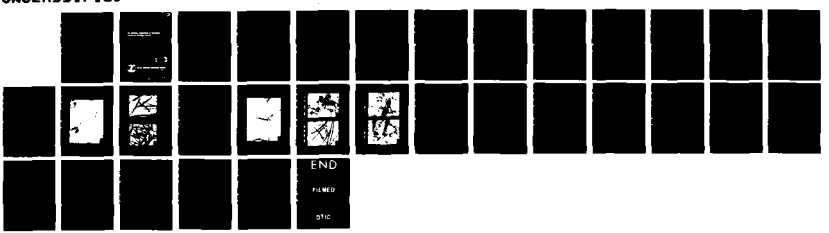

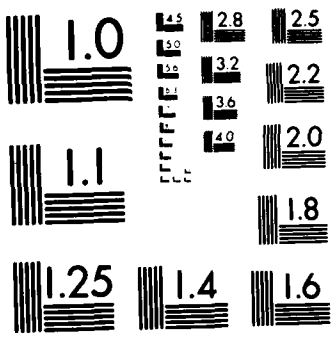

NSWC TR 82-416

AD-A148 673

THE PHYSICAL PROPERTIES OF THE SILICA COMPOSITE SINTERED PLASMA

BY W. A. FERRANDO W. W. LEE A. L. LEE S. A. SPIGLA

RESEARCH AND TECHNOLOGY DEPARTMENT

DECEMBER 1982

Approved for public release, distribution unlimited

DTIC FILE COPY

DTIC ELECTE DEC 2 8 1984 S D E

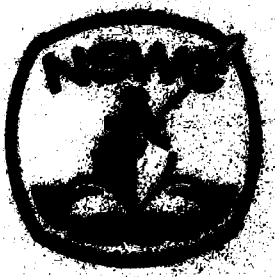

NAVAL SURFACE WEAPONS CENTER

Dahlgren, Virginia 22448 • Silver Spring, Maryland 20910

84 12 12 008

UNCLASSIFIED

SECURITY CLASSIFICATION OF THIS PAGE *(When Data Entered)*

REPORT DOCUMENTATION PAGE		READ INSTRUCTIONS BEFORE COMPLETING FORM
1. REPORT NUMBER NSWC TR 82-416	2. GOVT ACCESSION NO. AD-A148 673	3. RECIPIENT'S CATALOG NUMBER
4. TITLE *(and Subtitle)* PHYSICAL PROPERTIES OF THE NICKEL COMPOSITE SINTERED PLAQUE		5. TYPE OF REPORT & PERIOD COVERED INTERIM TECHNICAL REPORT '81, '82 6. PERFORMING ORG. REPORT NUMBER
7. AUTHOR(s) W. A. Ferrando, W. W. Lee, A. L. Lee, and R. A. Sutula		8. CONTRACT OR GRANT NUMBER(s)
9. PERFORMING ORGANIZATION NAME AND ADDRESS Naval Surface Weapons Center (Code R32) White Oak Silver Spring, MD 20910		10. PROGRAM ELEMENT, PROJECT, TASK AREA & WORK UNIT NUMBERS 62761N; F61545; SF61-545-601; 2R32BH
11. CONTROLLING OFFICE NAME AND ADDRESS		12. REPORT DATE December 1982 13. NUMBER OF PAGES 32
14. MONITORING AGENCY NAME & ADDRESS*(if different from Controlling Office)*		15. SECURITY CLASS. *(of this report)* UNCLASSIFIED 15a. DECLASSIFICATION/DOWNGRADING SCHEDULE

16. DISTRIBUTION STATEMENT *(of this Report)*

Approved for public release; distribution unlimited.

17. DISTRIBUTION STATEMENT *(of the abstract entered in Block 20, if different from Report)*

18. SUPPLEMENTARY NOTES

19. KEY WORDS *(Continue on reverse side if necessary and identify by block number)*

Sintered plaque
Composite plaque
Plaque resistivity
Nickel plaque
Nickel electrode
Plaque resistivity
Composite electrodes

20. ABSTRACT *(Continue on reverse side if necessary and identify by block number)*

The nickel composite plaque is a new concept in sintered substrates for application in alkaline energy storage systems. The plaque is fabricated from nickel coated graphite fibers which, upon sintering in reducing atmosphere, produces a strong lightweight structure of open porosity suitable for electrode use.

The four test areas of this report include: tensile strength, porosity, electrical resistivity and SEM micrography of the plaque structure.

DD FORM 1 JAN 73 1473 EDITION OF 1 NOV 65 IS OBSOLETE
S/N 0102-LF-014-6601

UNCLASSIFIED

SECURITY CLASSIFICATION OF THIS PAGE *(When Data Entered)*

20. (Cont.)

Porosities of 55 to over 90 percent void volume are achievable with the composite plaques, while maintaining structural integrity. Porosimetry measurements indicate approximately a 4X greater than mean pore size and 1.5X broader pore size distribution than commercial powder sinter. Tensile strengths were measured as a function of nickel coating thicknesses. A strength of 75-85kg/cm^2 was observed for plaques with fiber nickel coating thickness of about 1μ. Electrical resistivities of 400-600μ·Ω·cm were measured for plaques 1.0mm thick fabricated from fibers with 0.6-1.0μ thick nickel coating.

FOREWORD

This report explores some of the important physical parameters of the fiber composite nickel plaque under development at NSWC. Results from electrical resistivity, tensile strength, porosity by standard measurement techniques and plaque structure provided by scanning electron micrography have shown that lightweight, durable, and energy efficient electrodes can be fabricated.

Comparison with a high quality commercial nickel sintered plaque shows acceptable performance of the composite in every area. Moreover, a considerable range of overlap with parameter values common in powder sinters exists for the composite. This allows an excellent opportunity to optimize the latter for specific requirements. In addition to being lightweight, the composite plaques possess the desirable feature of a highly open, interconnected structure which is easily impregnated with active material.

The authors express their appreciation to Dr. M. K. Norr of the center for his fine work in providing the SEM photographs.

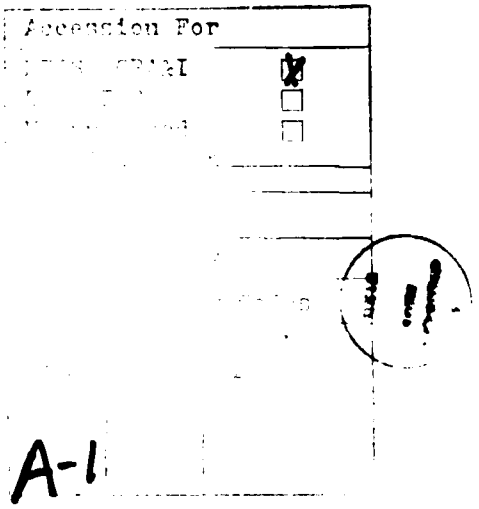

Approved by:

J. R. Dixon

JACK R. DIXON, Head
Materials Division

CONTENTS

ILLUSTRATIONS

TABLES

INTRODUCTION

A new concept in sintered plaque fabrication for use in electrode production for nickel alkaline battery systems is the nickel composite plaque.[1] This plaque is made from highly graphitized carbon pitch mat fibers, coated with electroless nickel, compressed around a grid and sintered in a reducing (H_2) atmosphere. The result is a strong lightweight sintered composite structure of open porosity suitable for use in various battery electrodes.

This report discusses the physical properties of this composite plaque material. These results have been derived from tests on only two sets of plaques and, therefore, must not be considered exhaustive. The reported data establishes an acceptable baseline for the composite plaque which can be compared to that of powder sintered plaques. The four test areas include tensile strength, porosity, resistivity and SEM micrography of the plaque structure.

EXPERIMENTAL PROCEDURE

Sintered nickel plaques have been the substrate of choice for many years as a medium for incorporation of electrochemically active material in secondary alkaline battery systems, where high rate capability and durability are important. Such plaques have been made conventionally by sintering a fine nickel powder.[2] They have the advantage of providing a highly conductive and porous substrate for containing the active species. Their disadvantages include weight and material/fabrication costs. The nickel composite plaque addresses these factors. The composite plaque is made by coating a graphite fiber mat (Thornel Type "P" VMA Grade, Union Carbide Corp.) using an electroless nickel solution (Allied-Kelite, Richardson Chemical Company). The nickel coated fiber is placed under compaction pressure around a current collection grid and sintered in a reducing (H_2) atmosphere.

All composite plaques used in this study were made from available graphite mat containing fibers approximately 7-17μ in diameter ($1\mu = 10^{-6}$ meter).

The electroless nickel coating, containing 2 to 10 percent phosphorous, has a eutectic point near 840°C. Sintering, therefore, must be carried out below this temperature to prevent the eutectic liquid from forming and running off the fibers during the process. A 2 hour sintering time is used, although based upon experience with powder sinters,[2] a period of 15 to 20 minutes is probably sufficient.

An initial set of plaques was sintered at 762°C and 812°C as a function of compaction pressure to assess the integrity of the fiber sinter bonds. A second set of plaques, containing the same amount of graphite fiber, was sintered as a function of nickel coating thickness to determine the effect of the nickel coating on the physical properties of the plaque. Typical data on the second plaque set is given in Table 1. This consisted of plaques produced with (nominal) nickel coating thicknesses of 0.3 to 1.5μ and plaque thicknesses of .75, 1.0, and 2.5mm, containing pure nickel expanded mesh current collectors. For comparison, a series of 1.0mm thick plaques, made without the current collector grid, is included. Finally, a 0.70mm thick commercial sinter was measured for reference.

POROSITY

Porosity measurements were made by water imbibition. Figure 1 shows the dependence of porosity on nickel coating thickness for the 0.75 and 1.0mm plaques at constant fiber content of 2.1 and 2.6 grams respectively. A variation of about 15 percent is observed in porosity as a function of nickel coating thickness.

Porosities of 55 percent to 95 percent have been produced in the composite plaques by varying the degree of compaction pressure (plaque thickness) for a given fiber content prior to sintering. Plaques fabricated with nickel coatings less than 0.5μ thick tend toward structural weakness, blistering and fiber separation. These problems, however, are caused by inadequately coated portions of fiber resulting from non-uniformity due to hand processing. Composite plaques of good quality were obtained with nickel coating thicknesses in the range of 0.6 to 0.9μ.

PLAQUE PORE SPECTRUM BY MERCURY INTRUSION POROSIMETRY

The mercury intrusion porosimeter method produces data on the volume of mercury forced into a porous sample as a function of applied pressure. By computing the appropriate derivative $\Delta VHg/\Delta P$, the fractional porosity versus effective pore diameter is obtained. Figures 2(a) and 2(b) show the results of such measurements on a powder sinter and composite plaque, respectively.

TABLE 1. COMPOSITE PLAQUE PARAMETERS

Plaque Thickness mm(nom.)	Coating Thickness μ (nom.)	Porosity %	Resist-ivity μΩcm	Tensile Strength kg/cm^2	Dry Weight grams	Mean Pore Diameter μ
0.75	0.3	88	673	36*	5.9	-
0.75	0.6	81	545	62*	7.8	-
0.75	0.9	75	434	72*	10.9	-
0.75	1.5	73	348	69*	13.9	-
1.0	0.3	95	869	3.5	6.4	-
1.0	0.6	86	650	48*	8.1	-
1.0	0.9	79	517	50*	11.0	-
1.0	1.5	79	430	69*	13.7	-
1.0 w/o grid	0.3	94	4228	12	3.6	66.0

* Average of two runs
** Manufacturer spec
† Crack observed in sinter
∇ Grid break

TABLE 1. (Cont.)

Plaque Thickness mm(nom.)	Coating Thickness μ (nom.)	Porosity %	Resistivity μΩcm	Tensile Strength kg/cm^2	Dry Weight grams	Mean Pore Diameter μ
1.0 w/o grid	0.6	83	1325	42	7.5	59.5
1.0 w/o grid	0.9	80	976	59	9.2	60.0
1.0 w/o grid	1.5	77	586	77	12.9	56.5
2.5	0.3	73	1578	19	13.7	-
2.5	0.6	80	1008	78	18.1	-
2.5	0.9	74	807	72	23.4	-
0.70 powder	-	84*	140	44† 121∇	14.1	15.0

* Average of two runs
** Manufacturer spec
† Crack observed in sinter
∇ Grid break

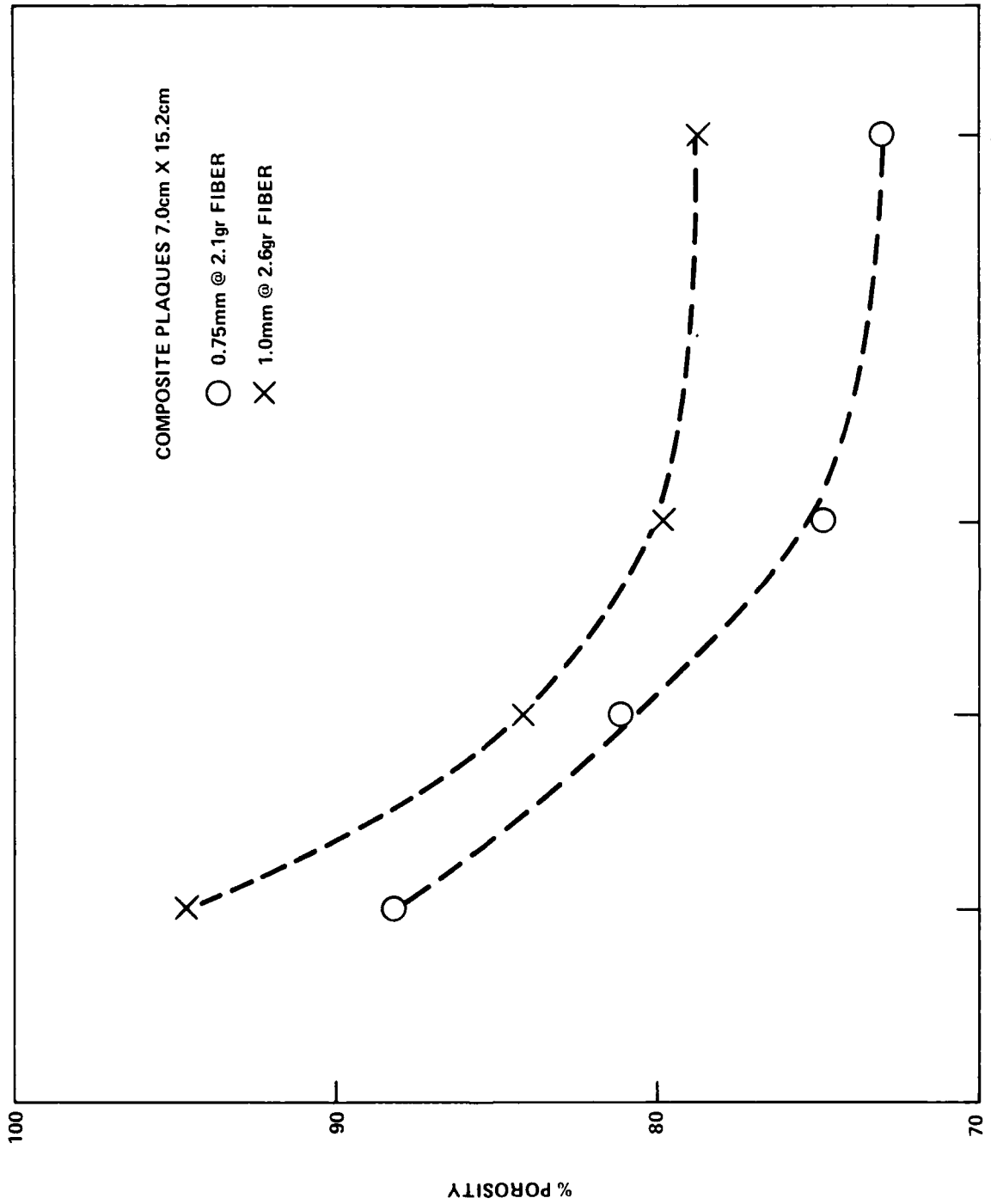

FIGURE 1. PLAQUE POROSITY VERSUS NICKEL COATING THICKNES [illegible] NT FIBER CONTENT

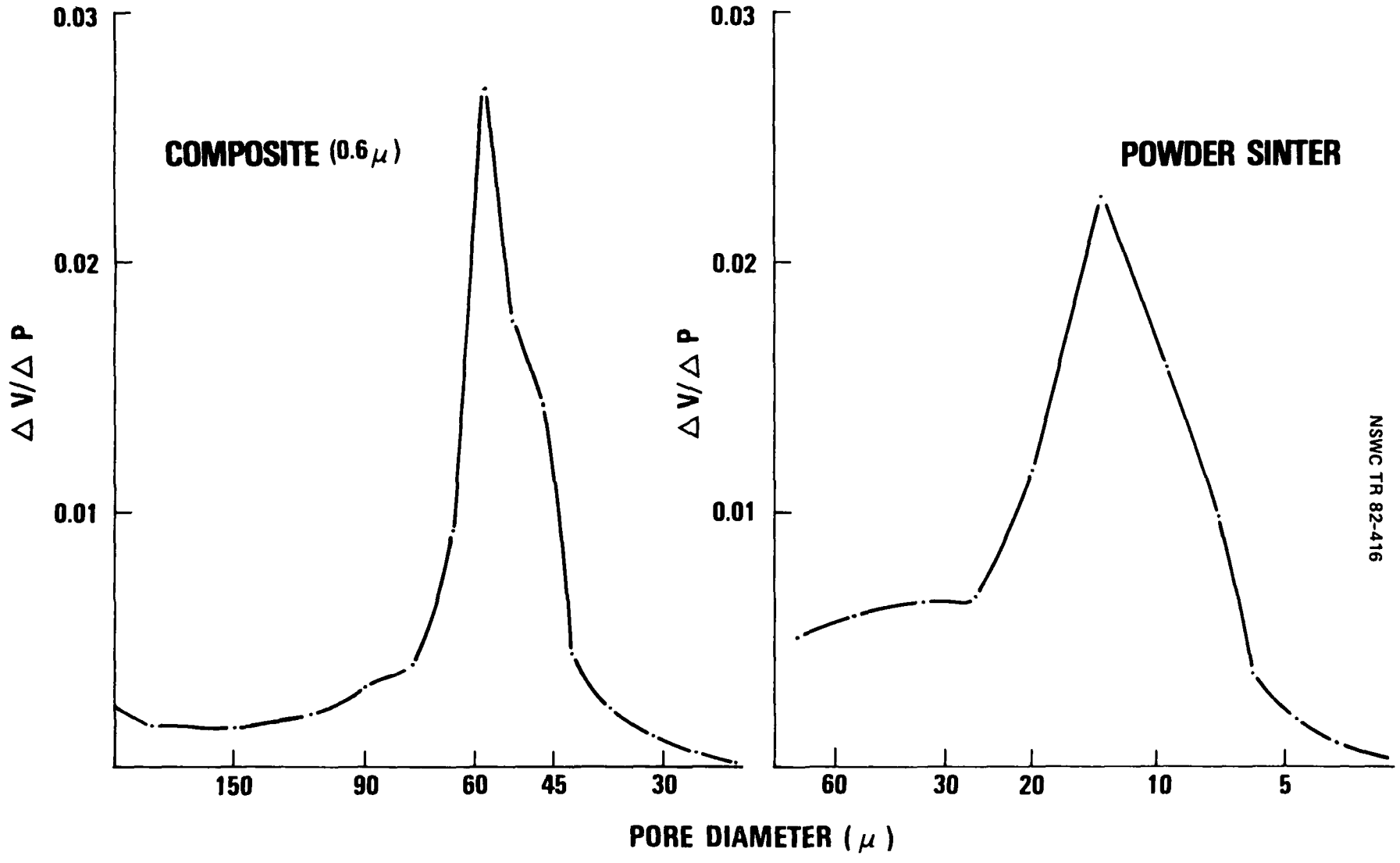

FIGURE 2. PLAQUE PORE SPECTRUM BY MERCURY INTRUSION POROSIMETRY

The number of pores of effective diameter indicated along the log axis is proportional to the curve height. The figures have a roughly similar shape with the maximum void volume occurring at about 15μ for the powder sinter and 60μ for the composite plaque. The porosity distribution is about 50 percent broader in the latter. As the nickel coating thickness is varied from 0.3 to 1.5μ, the pore size distribution maximum shifts from 66μ to 56μ. These data quantify the pore size difference between the composite and typical powder plaque. For practical purposes the pores are considered spherical cavities. While this is far from the true topography of composite sinters, it is a convenient construct for cavity size comparisons.

The pore size versus nickel coating thickness dependence is not strong, as noted above. The 20 percent or so difference in pore size between plaques of thin and thick nickel coating is not likely to affect impregnation/formation conditions significantly. Of primary importance, however, is the 4X larger average pore size of the composite compared with powder sinters. The larger pores of the former may produce an electrode with some characteristics of the pocket plate. This implies some reduction in efficiency at high rate discharge compared with that of a powder sinter of equal thickness. Preliminary tests indicate that the composite plaque suffers a 5-10 percent penalty in active material utilization level compared with that typical of powder sinters. At this stage, the reduced utilization cannot be attributed reliably either to the larger pore size or marked differences in morphology between the composite and powder sinters. New, uniformly coated fibers of constant smaller diameter are becoming available. These will produce plaques of smaller, more uniform pore size, which will more closely match the pore size and surface area of the powder sinters.

SCANNING ELECTRON MICROSCOPIC STUDY

SINTER BOND STRENGTH

SEM photography is a powerful tool in examining sinter bonding, active material deposition, changes in morphology, etc. Figure 3 shows a portion of an impregnated plaque which has been cut and examined on edge. The stress of cutting has pulled apart two fibers at a sinter point, revealing the integrity of the sinter bond. This indicates the potential durability of the composite plaque under the physical and chemical stresses of cycling. The long-term plaque cycling test discussed below revealed that, although the nickel coating had considerably degraded, there was no evidence of disproportionate failure of the sinter bonds.

PLAQUE DURABILITY

Two tests of plaque durability were made. In the first, a portion of composite plaque was immersed in 31 percent KOH electrolyte at 75°C for 2 months with no applied potential. Figures 4(a) and 4(b) show this sample before and

FIGURE 3. SEM PHOTOGRAPH OF FRACTURED SINTER BOND

(a)

(b)

FIGURE 4. SEM PHOTOGRAPH OF COMPOSITE PLAQUE "CYCLED" 1000X

after immersion. No major corrosive attack is evident. Therefore, plaque deterioration does not occur under open circuit conditons in the electrolyte. This result implies a potentially long "shelf" life of the composite electrode.

The second test involved long term alternating anodization (charge) and cathodization (discharge) periods at moderate current density, equivalent to 1000 cycles. Figure 5 shows the plaque after this test. It remains intact although the surface has assumed an eroded appearance. Oxidation of the nickel coating produced the equivalent of about 7 percent the utilization of a fully impregnated electrode of similar dimensions. Some exposed and split fibers are evident, probably due to gradual electrolyte penetration. These oxidation and penetration processes will set the limit on composite plaque lifetime.

PLAQUE MORPHOLOGY

An estimate of pore size can be obtained from SEM photographs by measurement and comparison. Figures 6(a) and 6(b) show portions of composite plaque at 200X and powder sinter plaque at 1000X respectively. The contrast in morphology and pore size is evident. The composite is composed largely of wedge-shaped cavities arranged in an interconnected open structure. Sintering takes place at contact points of the randomly directed mat fibers. The powder sinter has generally smaller pore cavities. Sintering takes place along entire particle chains which aggregate to form cavities. A far greater number of sinter bonds are involved in forming the powder sinter plaque.

These SEM photographs do not give information on closed porosity. No systematic study in this area was attempted. Such an investigation will require several cross section photographs of an impregnated plaque to determine the presence of unimpregnated regions.

The mat fiber material used in the composite plaques has a specific surface area of $0.4 m^2$/gram, compared with an area of 0.25 to 0.5 m^2/gram for nickel powders after sintering. Therefore, due to a 2 to 2.5X greater mass/volume, powder sintered plaques have this factor advantage in pore surface area. Smaller surface area for a given porosity in the composite plaque implies larger average pore size.

Figures 7(a) and 7(b) show portions of the composite plaque after impregnation and after charge-discharge cycling, respectively. In Figure 7(a), the nickel composite electrode (Ni.C.E.) has been formed but not cycled. The active material (nickel hydroxide) is present as isolated lumps loosely bound within the pore cavities. After heavy cycling (>200) in a test cell, the active material has redistributed to conform to the cavity walls (Figure 7(b)). It has assumed a smooth, layered appearance with visible electrolyte flow channels. The active material apparently has optimized its electrical contact with the plaque. This is reflected in a marked increase (30 to 40 percent) in utilization between the initial and final states pictured in Figure 7. The sensitivity of electrode performance to plaque and active material morphology is aptly illustrated. Not only must the plaque have a large accessible pore surface area, but also the active material must be distributed to contact it intimately.

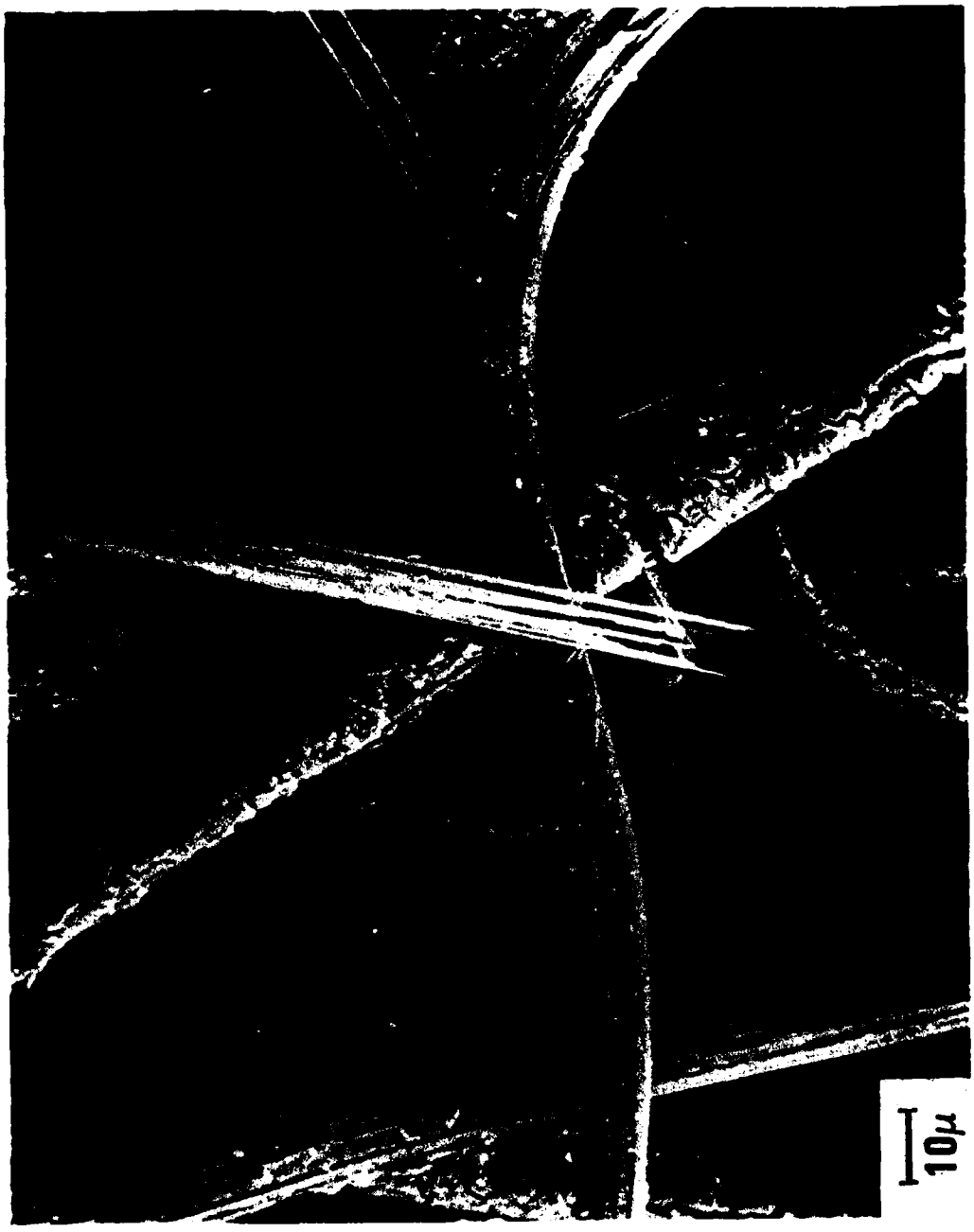

FIGURE 5. CORROSION RESISTANCE OF COMPOSITE PLAQUE IN ELECTROLYTE

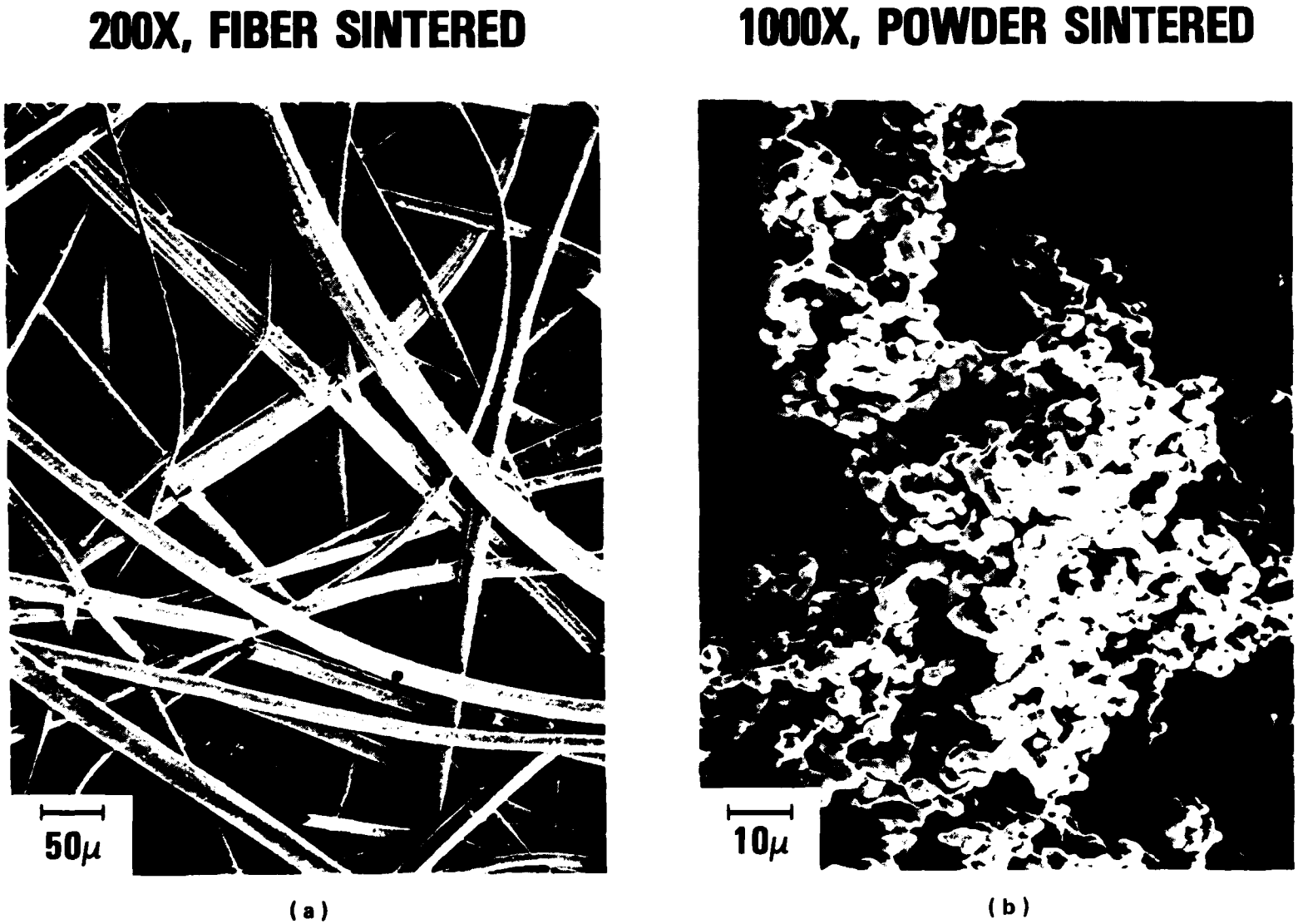

FIGURE 6. MORPHOLOGY, PORE SIZE COMPARISON COMPOSITE VERSUS POWDER SINTER

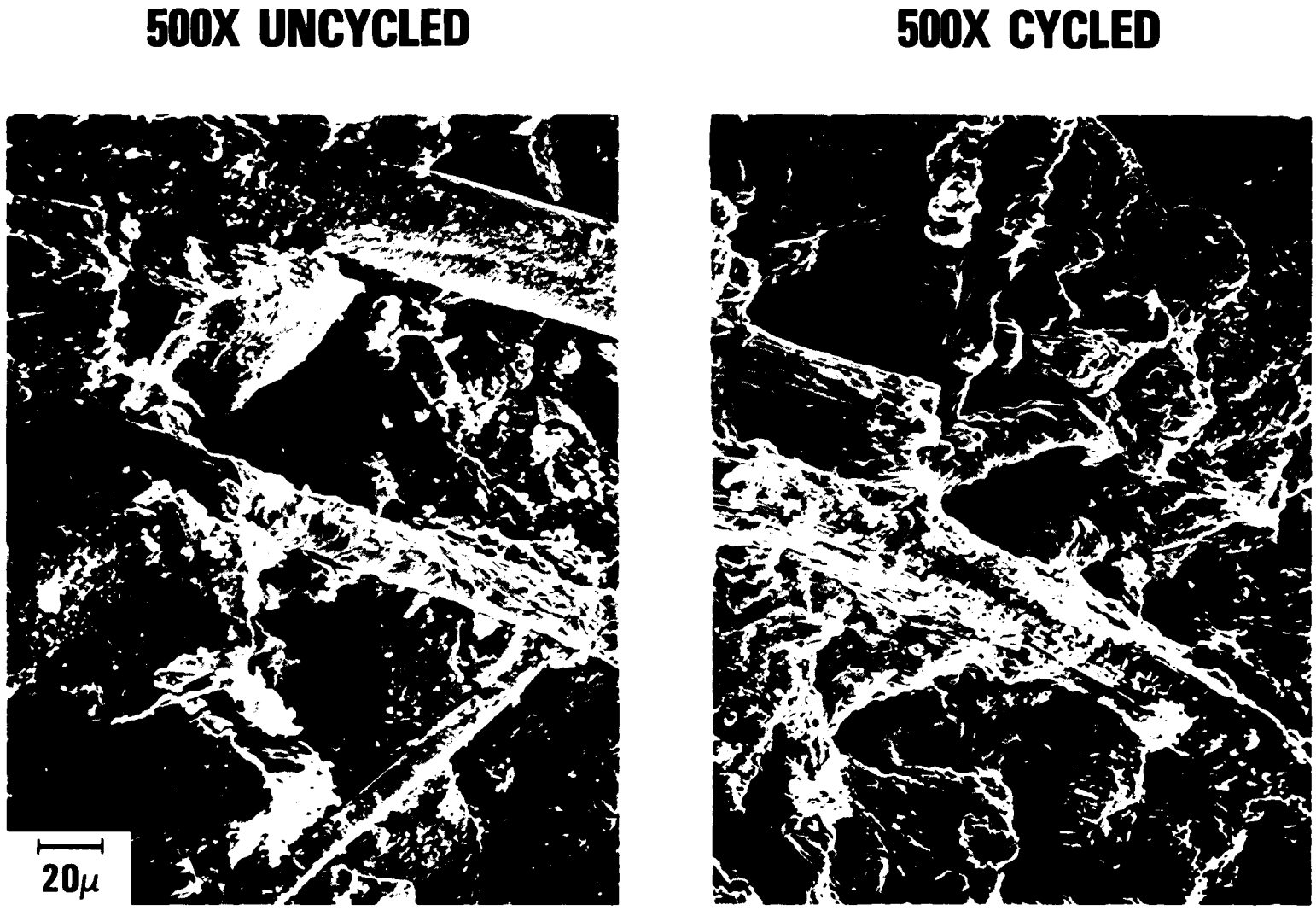

FIGURE 7. IMPREGNATED COMPOSITE PLAQUE DISTRIBUTION OF ACTIVE MATERIAL

ELECTRICAL RESISTIVITY

For maximum utilization of the active material and electrical efficiency of a cell to be achieved, the electrode resistivity should be a minimum. Of concern in sintered plate battery systems is the plaque resistivity, which is an important contributor to the cell's internal resistance.

Electrical resistivities of the composite test plaques were measured using a four point probe method. A known current is passed through the plaque. A potential probe of fixed width is used to measure the voltage drop across a plaque segment. Using the thickness and other information, the local resistivity is computed. Such measurements were made on the series of composite plaques sintered at 762°C and 812°C. Figure 8 shows the electrical resistivity versus compaction pressure for this series. The cross-hatched region indicates the resistivity range common in nickel powder sinters. The best results were obtained at 812°C, 0.63μ nickel coating.

Using this result as a baseline, a second set of plaques (Table 1) was fabricated and measured. Figure 9 displays the results of these measurements. Average plaque resistivity is plotted as a function of nickel coating thickness. Figure 9 shows that thin plaques have significantly lower resistivity than thick ones. For the same nickel coating thickness, a composite plaque 2.5mm thick has about twice the resistivity of one 0.75mm thick. The resistivity at each plaque thickness shows little decrease for coating thicknesses greater than about 0.6μ. The relatively lower resistivity of the thin plaques can be accounted for by the increased volume fraction occupied by the current collector (a pure nickel 0.15mm thick expanded metal grid) in the thin plates. A series of 1.0mm thick plaques was produced without the current collector grid in order to assess its contribution. The results are plotted as the upper curve of Figure 9. In the absence of the current collector, for a given nickel coating thickness, 1.0mm thick plaque has about twice the resistivity.

For comparison, the isolated point at lower right in Figure 9 indicates the measured resistivity of a recently manufactured 0.70mm thick powder sintered plaque. Its resistivity of 140μ•Ω•cm is about one-third that of a typical 0.75 to 1.0mm composite plaque of this series. Intersection with the practical resistivity range (~200 to 750μ•Ω•cm) determines the combinations of nickel coating and plaque thicknesses required for acceptable sinters. The data show that plaques thicker than 1.0mm will probably require heavier current collection grids to bring their resistivities within this range. If relatively thick nickel coatings are used, it might be possible to eliminate the current collector grid for some electrode applications.

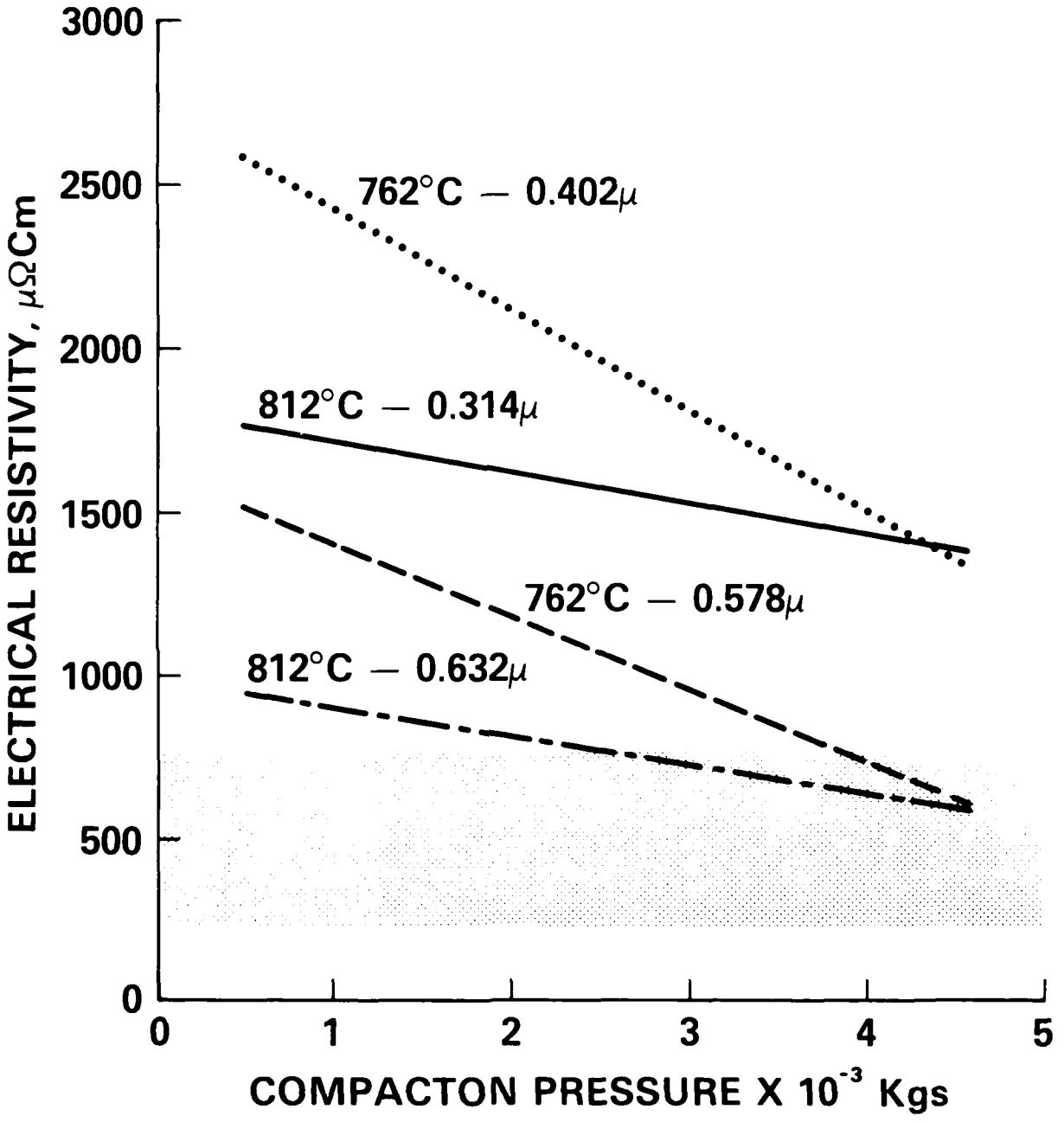

FIGURE 8. ELECTRICAL RESISTIVITY VERSUS COMPACTION PRESSURE

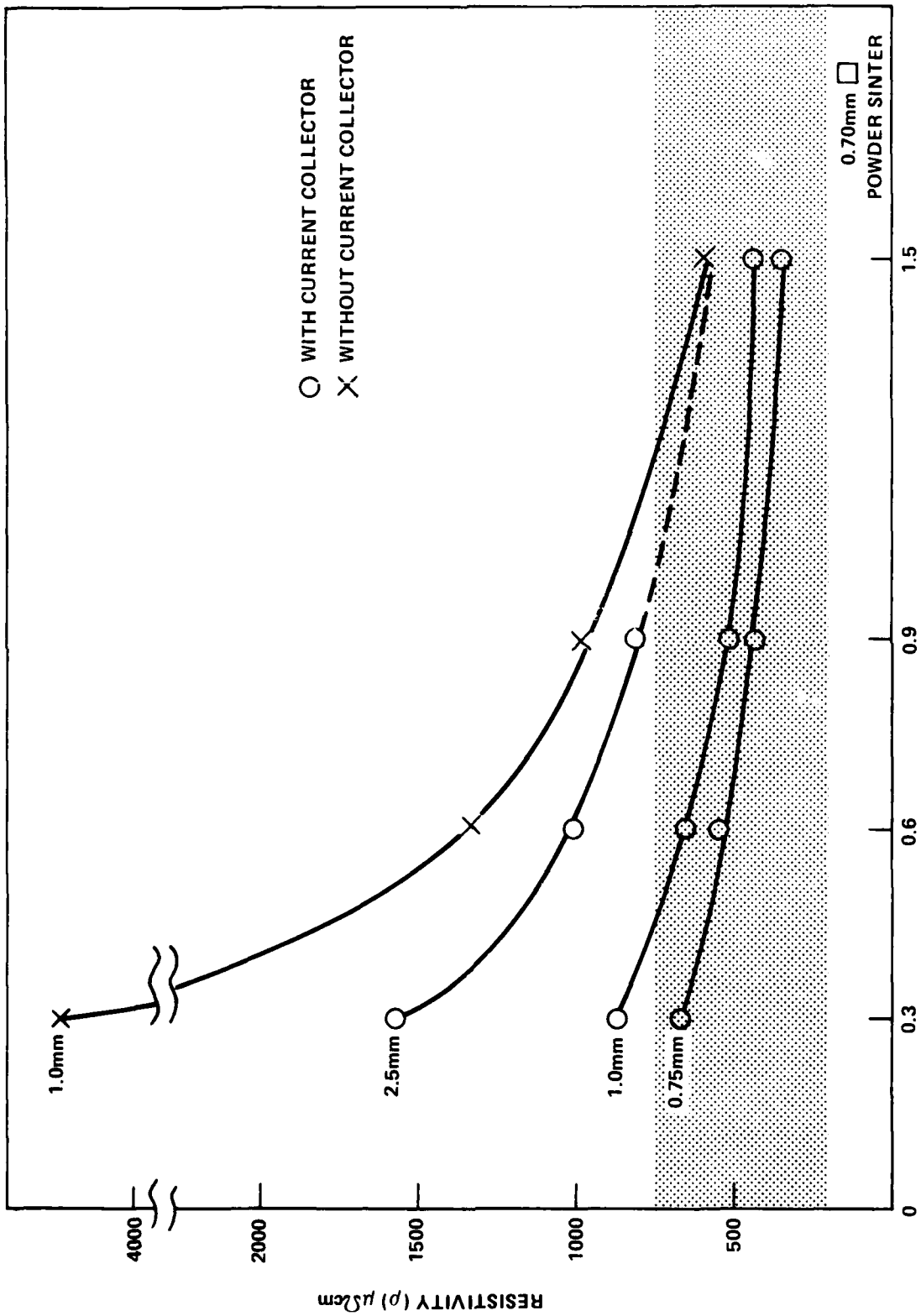

FIGURE 9. ELECTRICAL RESISTIVITY VERSUS NICKEL COATING THICKNESS

TENSILE STRENGTH

A simple test was used to determine the ultimate tensile strength of the composite plaques. The results were compared with those for powder sinters. The experimental arrangement used a hanging pedestal and weights to place the sample under static tension. The plaques were cut into strips of measured width. The only difficulty encountered was in devising a satisfactory holding method. Clamping the strip ends caused fiber damage and premature failure. The problem was solved by carefully epoxying small pieces of aluminum at each end of the strips. The test sample could then be placed conveniently under tension.

The load to failure (breakage) was recorded for each composite plaque sample of the first series. Figure 10 shows the failure load as a function of compaction pressure during sinter for various nickel coating thickness/ temperature combinations. The cross-hatch area indicates the range of tensile strengths obtained in powder sinters under normal processing conditions. The composite sinters processed at 800°C with 0.6μ nickel coating produced the best results.

A second set of composite sinters was tested. Failure strength as a function of nickel coating thickness is shown in Figure 11. Vertical bars indicate two measurements on the same plaque. The data show increasing strength up to a nickel coating thickness of about 0.9μ. Above this coating thickness, the ultimate tensile appears to become constant at 75 kg/cm^2. By constrast, from the data of Figure 10, increasing fiber content with compaction pressure translates into linear increase in tensile strength over the measured range. These data also show that tensile strengths greater than $75kg/cm^2$ are possible in the composite plaques by increasing their fiber content. However, a penalty will be paid in decreased porosity. The 0.70mm thick, recently manufactured, powder sinter plaque exhibited a crack in the sinter at about $45kg/cm^2$ as indicated in Figure 11. The ultimate tensile strength of $110kg/cm^2$ was due principally to its current collector grid strength rather than to the sinter body.

CONCLUSIONS

Porosity of the composite plaque may be varied over a wide range of 55 to >90 percent by altering its fiber content. The mean pore size of plaques subjected to testing was about 4X and width of distribution about 1.5X those of powder sinter plaques. The achievement of smaller pore size while maintaining high porosity in the composite plaques necessitates that a graphite material of somewhat smaller, more uniform fiber diameter be used.

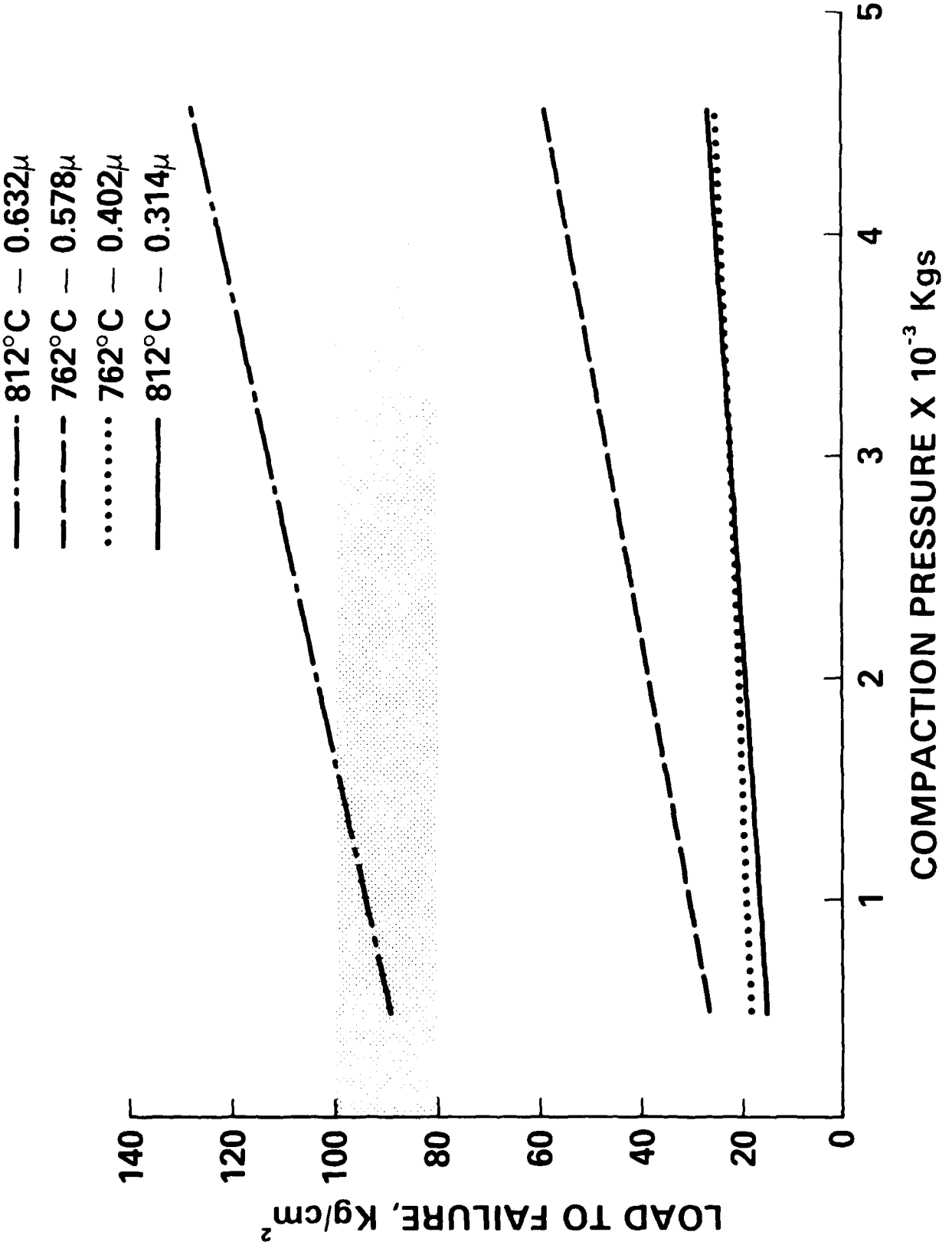

FIGURE 10. TENSILE STRENGTH VERSUS COMPACTION PRESSURE

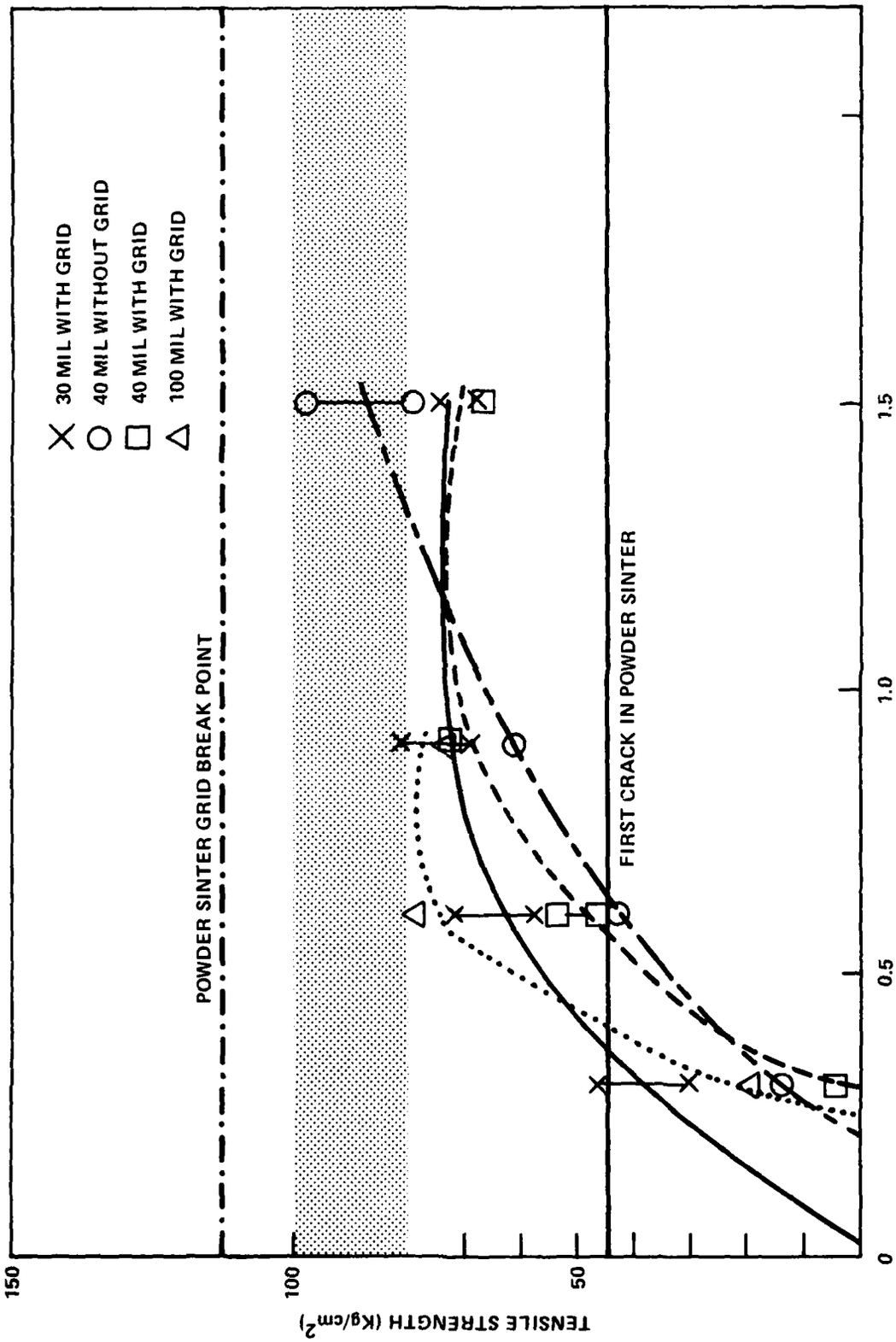

FIGURE 11. TENSILE STRENGTH VERSUS NICKEL COATING THICKNESS

SEM micrography confirms a composite plaque morphology of virtually 100 percent open interconnected porosity which readily accepts high active material impregnation levels. Micrographic observation of a cycled composite electrode indicates good intra-electrode electrolyte circulation.

The composite plaque electrical resistivity can be made comparable, by suitable nickel coating thickness, sinter temperature and fiber content, to that of typical powder sinters.

The ultimate tensile strength of the composite plaques increases with increasing nickel coating thickness, saturating at 75 to 85kg/cm^2 for nickel coating thicknesses around 0.9μ. The tensile load is carried by the composite fiber structure rather than by the nickel conductor grid.

Good durability was noted for the composite plaque against corrosion under long term immersion in hot KOH electrolyte. Stability against dissolution was demonstrated by the unimpregnated composite plaque under anodization (charge) with gas evolution and cathodization (discharge) conditions equivalent to 1000 cycles.

A sintering temperature of 800°C and nickel coating thickness of 0.6 to 0.9μ produce a composite plaque of suitable physical characteristics for cell use.

REFERENCES

1. Ferrando, W. A., and Sutula, R. A., "Lightweight Battery Electrode," U.S. Patent No. 4,215,190, 1980.

2. Falk, S. U., and Salkind, A. J., Alkaline Storage Batteries, (New York: John Wiley and Sons, Inc., 1969), p. 111.

DISTRIBUTION

	Copies
Defense Technical Information Center Cameron Station Alexandria, VA 22314	12
Defense Nuclear Agency Attn: Library Washington, DC 20301	1
Pentagon Project Officer, OSD(MRA&L)-WR Attn: William G. Miller Room 2B323 Washington, DC 20301	1
Office of Deputy Under Secretary of Defense for Research and Engineering Staff Specialist for Materials and Structures Attn: Mr. Jerome Persh Room 3D1089, The Pentagon Washington, DC 20301	1
Defense Advanced Research Projects Agency Attn: E. Van Reuth L. Jacobsen 1400 Wilson Boulevard Arlington, VA 22209	1 1
Institute for Defense Analyses R&E Support Division 400 Army-Navy Drive Arlington, VA 22202	1
Library of Congress Attn: Gift and Exchange Division Washington, DC 20540	4
Office of Chief of Naval Operations Operation Evaluation Group Washington, DC 20350	1
David W. Taylor Naval Ship Research and Development Center Attn: A. B. Neild (Code 2723) W. J. Levendahl (Code 2703) J. Woerner (Code 2724) H. R. Urbach (Code 2724) D. Icenhower (Code 2721) J. Gudas (Code 2813) W. Lukens (Code 2822) Annapolis Laboratory Annapolis, MD 21402	1 1 1 1 1 1 1
Naval Air Development Center Attn: Dr. E. McQuiller Dr. G. London Warminster, PA 18974	1 1
Naval Air Systems Command Attn: Mr. R. Schmidt (Code 52031A) Washington, DC 20361	1
Naval Electronic Systems Command Attn: A. H. Sobel (Code PME 124-31) Washington, DC 20360	1
Naval Intelligence Support Center Attn: Dr. H. Ruskie (Code 362) 4301 Suitland Road Washington, DC 20390	1

DISTRIBUTION (Cont.)

	Copies
Naval Material Command	
Attn: Code 08T223	1
J. Kelly (MAT 0725)	1
W. Holden (MAT 08E4)	1
O. J. Remson (MAT 071)	1
G. R. Spaulding (MAT 072)	1
Washington, DC 20360	
Naval Ocean Systems Center	
Attn: Code 922	1
Dr. S. D. Yamomoto (Code 513)	1
P. D. Burke (Code 9322)	1
San Diego, CA 92152	
Naval Ordnance Station	
Attn: Howard R. Paul	1
Project Manager	
Southside Drive	
Louisville, KY 40150	
Naval Postgraduate School	
Attn: Dr. William M. Tolles (Code 612)	1
Monterey, CA 93940	
Naval Research Laboratory	
Attn: Dr. Fred Saalfeld (Code 6100)	1
A. Simon (Code 6130)	1
S. C. Sanday (Code 6370)	1
I. Wolock (Code 8433)	1
H. Chaskelis (Code 8431)	1
4555 Overlook Avenue, S.W.	
Washington, DC 20375	
Naval Sea Systems Command	
Attn: M. Kinna (Code 62R4)	1
J. DeCorpo	1
E. J. Anderson	1
Code 5433	1
H. Vanderveldt (Code 05R15)	1
Code 99612	2
Code 0841B	1
Washington, DC 20362	
Naval Underwater Systems Center	
Attn: J. Moden (Code 36123)	1
R. Lazar (Code 36301)	1
Newport, RI 02841	
Naval Weapons Center	
Attn: A. Fletcher (Code 3852)	1
China Lake, CA 93555	
Naval Weapons Support Center	
Attn: M. Robertson	1
Electrochemical Power Sources Division	
Crane, IN 47522	
Office of Naval Research	
Attn: G. Neece (Code 413)	1
B. MacDonald (Code 471)	1
G. Sandoz (Code 715)	1
J. Smith (Code 413)	1
800 N. Quincy Street	
Arlington, VA 22217	
Strategic Systems Project Office	
Crystal Mall No. 3	
Attn: G. Needham (Code 273)	1
LCDR F. Ness (Code 234)	1
LCDR H. Nakayama (Code 272)	1
Washington, DC 20362	
Army Electronics Research and Development Command	
Attn: A. Legath (Code DELET-P)	2
S. Gilman (Code DRSEL-TL-P)	1
E. Brooks (Code DRSEL-TL-P)	1
G. DiMasi (Code DRSEL-TL-P)	1
Fort Monmouth, NJ 07703	
Army Foreign Science and Technology Center	
Attn: J. F. Crider (Code FSTC/DRXST-MTI)	1
220 7th Street	
Charlottesville, VA 22901	

DISTRIBUTION (Cont.)

	Copies
Army Materials & Mechanics Research Center	
Attn: J. J. DeMarco	1
J. W. McCauley	1
A. Levitt	1
J. Greenspan	1
F. Larson	1
L. R. Aronin	1
Watertown, MA 02172	
Army Material Development and Readiness Command	
Attn: J. W. Crellin (Code DRCDE-L)	1
5001 Eisenhower Avenue	
Alexandria, VA 22333	
Army Mobility Equipment R&D Command	
Attn: J. Sullivan (Code DRXFB)	1
G. D. Farmer, Jr. (Code DRDME-VM)	1
Dr. J. R. Huff (Code DRDME-EC)	1
Electrochemical Division	
Fort Belvoir, VA 22060	
Army Research Office	
Attn: B. F. Spielvogel	1
J. C. Hurt	1
P.O. Box 12211	
Research Triangle Park, NC 27709	
Army Scientific Liaison & Advisory Group	
Attn: HQDA (DAEN-ASR-SL)	1
Washington, DC 20314	
Ballistic Missile Defense Officer	
BMD-ATC	
Attn: M. L. Whitfield	1
P.O. Box 1500	
Huntsville, AL 35807	

	Copies
Office of Chief of Research & Development	
Attn: Dr. S. J. Magram	1
Department of the Army	
Energy Conversion Branch	
Room 410, Highland Building	
Washington, DC 20315	
Air Force Flight Dynamics Laboratory	
Attn: D. Roselius	1
L. Kelley	1
Wright-Patterson Air Force Base	
Dayton, OH 45433	
AF Weapons Laboratory	
Attn: Charles Stein	1
Kirtland AFB	
Albuquerque, NM 87115	
Air Force Wright Aeronautical Laboratory	
Attn: M. Duhl (Code MB)	1
T. Ronald (Code LLS)	1
W. S. Bishop (Code POOC-1)	1
R. M. Neff (Nonmetellic Mat. Div.)	1
D. R. Beeler (Code MB)	1
D. Marsh (Electrochemistry Code POOC-1)	1
Wright-Patterson AFB, OH 45433	
Frank J. Seiler Research Laboratory, AFSC	
Attn: LTCOL Lowell A. King (Code FJSRL/NC)	1
USAF Academy, CO 80840	
SD/YLXT	
Attn: MAJ R. Gajewski	1
P.O. Box 92960, WPC	
Los Angeles, CA 90009	

DISTRIBUTION (Cont.)

	Copies
Central Intelligence Agency	
Attn: C. Scuilla	1
G. Methlie	1
Washington, DC 20505	
Department of Energy	
Attn: Dr. A. Landgrebe (Code MS E-463)	1
Division of Applied Technology	
Washington, DC 20545	
Department of Energy	
Attn: L. J. Rogers (Code 2101)	1
Division of Electric Energy Systems	
Washington, DC 20545	
NASA Scientific and Technical Information Facility	
Attn: Library	1
P.O. Box 33	
College Park, MD 20740	
National Bureau of Standards	
Metallurgy Division	
Inorganic Materials Division	1
Washington, DC 20234	
NASA Lewis Research Center	
Attn: Mr. R. A. Signorelli	1
J. S. Fordyce (Code MS 309-1)	1
H. J. Schwartz (Code MS 309-1)	1
Cleveland, OH 44135	

	Copies
General Electric Company	
Re-entry Systems Operations	
Attn: K. J. Hall	1
P.O. Box 7722	
Philadelphia, PA 19101	
NASA Goodard Space Flight Center	
Attn: G. Halpert (Code 711)	1
Greenbelt, MD 20771	
NASA Headquarters	
Attn: M. Greenfield (Code RTS-6)	1
Dr. J. H. Ambrus	1
600 Independence Avenue	
Washington, DC 20546	
NASA/Langley Research Center	
Attn: E. Mathauser (Code MS188A)	1
Dr. T. Bales	1
Dr. D. Tenney	1
Hampton, VA 23365	
Ms. A. L. Lee	
3004 Castleleigh Road	
Silver Spring, MD 20904	1
Internal Distribution:	
E431	9
E432	3
R04 (D. L. Love)	1
R30 (J. R. Dixon)	1
R32 (R. A. Sutula)	1
R32 (W. A. Ferrando)	10
R32 (Staff)	5
R32 (W. W. Lee)	1
R33 (C. E. Mueller)	1

END

FILMED

1-85

DTIC